Latin American Journal of Solids and Structures
www.lajss.org

Ductility Analysis of RC Beams Considering the Concrete Confinement Effect Produced by the Shear Reinforcement: a Numerical Approach

Abstract

In this paper, a simplified numerical approach to study the influence of the confinement effect provided by transversal reinforcement on the ductility behavior of RC beams in bending is proposed. A unidimensional FEM mechanical model coupled to the Mazars' damage model to simulate concrete behavior was adopted to assess ductility curvatures at the ultimate limit state. The confinement effect was incorporated to the numerical model through a calibration process of the damage internal parameters, based on the Least Square Method and an analytical law proposed by Kent and Park (1971). Several numerical analyses were carried out considering different designs of RC beams according to a parametric study varying the neutral axis position, concrete compressive strength and the volumetric transversal reinforcement ratio. The obtained results showed the importance of the amount of transversal reinforcement on the ductility behavior, increasing the ductility factor even for the cases with inappropriate neutral axis position.

Keywords

RC beams, finite element; ductility; confinement; concrete; damage.

Caio Gorla Nogueira [a, *]
Isabela Durci Rodrigues [b]

[a] Department of Civil Engineering, São Paulo State University – UNESP/FEB, Brazil - cgnogueira@feb.unesp.br
[b] Department of Civil Engineering, São Paulo State University – UNESP/FEB, Brazil - isabela.dr@hotmail.com

[*] Corresponding Author

http://dx.doi.org/10.1590/1679-78253904

Received 07.04.2017
In revised form 11.08.2017
Accepted 28.08.2017
Available online 18.09.2017

1 INTRODUCTION

Nowadays, reinforced concrete (RC) structures are largely used in engineering works from small constructions to tall buildings and bridges. The possibility to build any kind of geometry and format for the structural systems have given to reinforced concrete the status of general construction material. The costs associated to the construction of the buildings and other structures are still competitive when compared to several materials. Furthermore, RC as a structural material, especially when used for example in statically indeterminate structures, gives to the elements the capac-

ity to behave according to the assumptions specified by the designer of the structural system, since the designing and execution of the structure respect the design hypothesis, limitations imposed by the codes and good procedures *in situ*. Regarding to the RC beams, the most part of these structural elements is designed to support bending moments and shear forces that come from the external loads. But, in general, the bending moment effects are more important than the shear ones, especially when the beams have higher values of the span-to-depth ratio, in which the shear strains can be neglected and the Euler-Bernoulli's hypothesis governs the overall structural behavior and mainly the ultimate strength of those elements.

Among many aspects required in RC beams and slabs design, ductility has become mandatory by the standard codes (ABNT NBR 6118: 2014; EUROCODE 2: 2004; ACI 318: 2002). In this context, ductility can be defined as the ability to support large plastic deformations before failure without significant resistance loss. The main reasons to consider ductility as a mandatory characteristic in the modern structural design are: ductility prevents brittle ruptures, which is a failure mode that must always be avoided; elements with ductile behavior have higher plastic rotation capacities when compared to brittle elements and contribute to large deformations/displacements before a physic rupture (Ko et al. 2001); ductility of cross sections are essential to provide bending moment redistribution along the beam as longitudinal reinforcement steel yields ensuring the redundant behavior of hyperstatic structures (Kara and Ashour 2013). Another important application in which the ductility is essential to guarantee safe behaviors of RC structural systems is related to dynamic loads generated by seismic tremors. In such cases, the ductility of the structural elements must be predicted and quantified in a detailed way to avoid severe damage and brittle failures of the buildings (Lopes et. al 2012; Arslan 2012; Demir et al. 2016).

However, the prediction and the assessment of ductility as a single value to describe how ductile or brittle is an element or some cross section is not an easy task. There are several parameters interacting each other that influence the ductility at ultimate limit states. Moreover, it is impossible to dissociates ductility from rigidity of a RC element because they are function of almost the same parameters as: longitudinal reinforcement ratio, concrete strength, concrete softening branch in compression, crack pattern development, tension stiffening, bond-slip relationship (Lee and Pan 2003; Oehlers et al. 2009; Lopes et al. 2012). The curvature depends on the material strain levels and their limits. On the other hand, these strain values are function of the neutral axis position, which influences the effective depth and longitudinal reinforcement ratio.

In order to at least guarantee a ductile behavior for RC structural elements, the design codes impose some restrictions to the relative neutral axis position (β_x) on the cross section determinations. EUROCODE 2 (2004) and ABNT NBR 6118 (2014) recommend for ensure ductility in RC beams the following values: $\beta_x \leq 0{,}45$ for $f_{ck} \leq 50$ MPa and $\beta_x \leq 0{,}35$ for $f_{ck} > 50$ MPa at ultimate limit state. Therefore, when the codes adopt those recommendations for the neutral axis position, the balanced condition, in which $\beta_x = 0{,}628$ (limit between domains 3 and 4), is no longer accepted because it can lead to a brittle failure (Araújo 2009). Although this form to solve the problem of ductility is simple and intuitive, it does not quantify the ductility of the designed RC cross sections. Moreover, several important mechanisms that interfere on the overall behavior of the RC beams are not take into account, such as the evolution of damage along time as the loading conditions change;

confinement effect of the compressed concrete provided by stirrups and tension stiffening (Oehlers et al. 2013).

Damage models (Mazars 1984; La Borderie 1991; Flores-Lopes 1993; Cervera et al. 1996) have been adopted successfully to represent the rigidity loss of the structural elements as a function of the loading conditions. In the most of damage models, the damage is defined by a scalar parameter that quantifies the local state of degradation and penalizes the material stiffness at that point. To perform the damage assessment, there are several constitutive models with their own assumptions and hypothesis about the starting and evolution of the damage. But as a general approach, damage models depend on the stress/strain state at a point (integration points localized along the finite elements) and an evolution criterion for damage. By adopting damage model approaches, the limitation on the EI values and its variation along the structural elements is overcome.

In the context of the absence of explicit quantification methods for ductility, Lee and Pan (2003) proposed an algorithm based on simplified analytical equations to RC beams designing considering that ductility factor as an input data. In their approach, the authors considered the Kent and Park's (1971) analytical model for concrete in compression to take into account the confinement effect caused by the transversal reinforcement. Daniell et al. (2008) studied the ductility in RC elements considering the plastic rotation capacity as a measure of ductility and associated it with ability to redistribute bending moments. Arslan (2012) carried out a parametric study varying some parameters listed in the design codes in order to ensure enough ductility for RC structures when subjected to earthquakes.

This paper presents a study about the influence of the confinement effect in RC beams ductility provided by shear reinforcement, considering a numerical approach via FEM. The confinement effect was incorporated to a unidimensional FEM mechanical model through a calibration procedure of the internal damage parameters adopted by the scalar Mazars' damage model. The calibration was carried out by a Nonlinear Least Square Method based on the Gauss-Newton strategy solution. Therefore, the effect of the confinement was automatically incorporated to the constitutive concrete compression law after concrete reach the stress $\times$ strain curve peak. The paper's main contribution is related to the use of a simplified numerical approach based on the calibration of the internal damage parameters taking into account the confinement effect. If the constitutive law of the material is known, the proposed procedure can be applied, which gives a general status to the model. A parametric analysis was carried out in a RC beam to study the effect of the confinement on the ductility, varying the neutral axis position, concrete strength and volumetric transversal reinforcement ratio.

2 THE MECHANICAL MODEL BASED ON FEM

2.1 Unidimensional Finite Element Approach

The studied structures in this paper are defined by RC beams considered as prismatic bar elements (one dimension) and represented only by their straight axis. In such way, the discrete approach adopted in the study is based on unidimensional finite element method. Figure 1 shows the frame plane 1D finite element used in the numerical analyzes and a generic example of discretization. Each element has 2 nodes and the nodal movement description is given by 3 degrees of freedom

(dof): 2 translational displacements (u and v in x' and y' respectively) and 1 rotation (θ in z), which implies in the total of 6 *dof* per element (3 per each node). Nogueira et al. (2013) presented the original formulation of the 1D finite element adopted here, which is based on the traditional displacement approach.

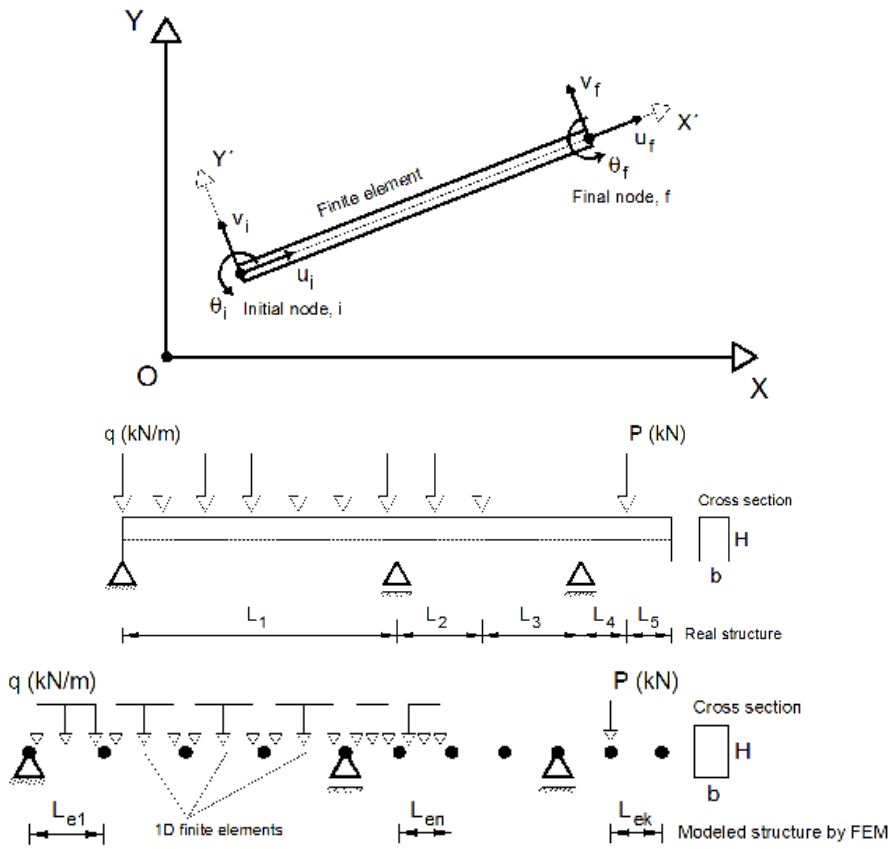


Figure 1: Frame plane 1D finite element and an example of discretization.

2.2 Isotropic Damage Model for Concrete

In general, concrete structures behavior is affected by crack formation and its growth as the external actions apply their effects over the elements. When cracks or any other type of micro defects increase on the element surface, there is stiffness loss and a damage parameter (D) can be associated to describe the concrete degradation state compared to the original intact state. In such way, the damage is expressed by the rate between the total area of all micro defects and the total intact area of the element. Several damage models were developed in the literature to take into account the concrete stiffness loss associated to loading process and crack evolution (Mazars 1984; La Borderie 1991; Cervera et al. 1996; Pituba 2003). In this study, a damage model proposed by Mazars (1984) was adopted to simulate the concrete behavior in tension and compression. The main hypothesis of the model can be resumed as: damage is scalar and an isotropic parameter; permanent strains are neglected; damage is due only by stretching states.

The effective second order stress tensor ($\overline{\boldsymbol{\sigma}}$) at the point can be defined by:

$$\overline{\boldsymbol{\sigma}} = \mathbf{C}:\boldsymbol{\varepsilon} \tag{1}$$

In which: C is the linear elastic fourth order constitutive tensor; ε is the second order strain tensor.

After the solution of the linear system of equations derived from the FEM, the strain tensor is achieved based on the nodal displacements for each integration point along the cross section of the element. Note that in the strain tensor there are the normal ($\varepsilon_x, \varepsilon_y, \varepsilon_z$) and shear ($\gamma_{xy}, \gamma_{yz}, \gamma_{xz}$) components which represent the entire state of strain. As one can define the strain tensor at each point of the element, the damage parameter can also be assessed for each integration point and it is used to evaluate the final effective stress later. Then, for each integration point, the eigenvalues of the strain tensor ($\varepsilon_1, \varepsilon_2, \varepsilon_3$) are obtained to analyze the degradation state as written below:

$$\boldsymbol{\varepsilon}^* = \begin{bmatrix} \varepsilon_1 & 0 & 0 \\ 0 & \varepsilon_2 & 0 \\ 0 & 0 & \varepsilon_3 \end{bmatrix} \tag{2}$$

The damage criterion used to verify the concrete integrity at each integration point can be given by:

$$f(\tilde{\varepsilon}, D) = \tilde{\varepsilon} - \hat{S}(D) < 0 \tag{3}$$

In which: $\tilde{\varepsilon}$ is the equivalent strain that represents the stretching state at the point; $\hat{S}(D)$ indicates the current threshold of the degradation state. In fact, this value controls the size of the damage surface, which expands when the equivalent strain reaches $\hat{S}(D)$.

In the beginning of the incremental-interactive process, $\hat{S}(D)$ receives the strain corresponding to the concrete peak stress (f_{tk}) in tension, which is $\varepsilon_{d0} = f_{tk}/E_c$. When the criterion described by Equation 3 is violated, $\hat{S}(D)$ is updated by the last value of the equivalent strain.
The equivalent strain assumes the form:

$$\tilde{\varepsilon} = \sqrt{\varepsilon_{1_+}^2 + \varepsilon_{2_+}^2 + \varepsilon_{3_+}^2} \tag{4}$$

The equivalent strain takes into account only the positive components of the main strain tensor ε^* because it reflects the hypothesis of the model that is damage is due only by stretching states.

The damage model of Mazars (1984) is defined by two independent damage parameters (D_T and D_C) to consider the non-symmetric behavior of concrete in tension and compression. After the assessment of each damage parameter, the final value of the damage (D) is given by the linear combination:

$$D = \alpha_T D_T + \alpha_C D_C \tag{5}$$

In which: α_T and α_C are weight factors to consider the importance in tension and compression of the strain state at the point. In cases of uniaxial tension, $\alpha_T = 1$ and $\alpha_C = 0$; uniaxial compression, $\alpha_T = 0$ and $\alpha_C = 1$; multiaxial states, the condition $\alpha_T + \alpha_C = 1$ must be respected.

A strategy, proposed by Perego (1990), was developed to evaluate such parameters and adopted in this work. The followed steps are written below and are applicable to each integration point along the cross section of the finite elements:

A) Evaluate the main strain tensor ($\boldsymbol{\varepsilon}^*$);

B) Evaluate the main stress tensor ($\boldsymbol{\sigma}^*$) by:

$$\boldsymbol{\sigma}^* = \mathbf{C}:\boldsymbol{\varepsilon}^* \tag{6}$$

A) Split $\boldsymbol{\sigma}^*$ into two parts, one positive (σ_+^*) and the other negative (σ_-^*) by:

$$\boldsymbol{\sigma}^* = \boldsymbol{\sigma}_+^* + \boldsymbol{\sigma}_-^* \tag{7}$$

B) Evaluate the positive ($\boldsymbol{\varepsilon}_+^*$) and negative ($\boldsymbol{\varepsilon}_-^*$) strain tensor by:

$$\begin{aligned} \boldsymbol{\varepsilon}_+^* &= \mathbf{C^{-1}}:\boldsymbol{\sigma}_+^* \\ \boldsymbol{\varepsilon}_-^* &= \mathbf{C^{-1}}:\boldsymbol{\sigma}_-^* \end{aligned} \tag{8}$$

After these steps, the weight factors can be given by:

$$\begin{aligned} \alpha_T &= \frac{\sum_{i=1}^{3}(\varepsilon_+^*)_i^+}{\varepsilon_+^V} \\ \alpha_C &= \frac{\sum_{i=1}^{3}(\varepsilon_-^*)_i^+}{\varepsilon_+^V} \end{aligned} \tag{9}$$

In which: $\mathbf{C^{-1}}$ corresponds to the inverse of the linear elastic fourth order constitutive tensor; $(\varepsilon_+^*)_i^+$ represents only the positive components of the positive strain tensor ($\boldsymbol{\varepsilon}_+^*$); $(\varepsilon_-^*)_i^+$ represents only the positive components of the negative strain tensor ($\boldsymbol{\varepsilon}_-^*$); ε_+^V is the strain value correspondent to the total stretching state at the point assuming the form:

$$\varepsilon_+^V = \sum_{i=1}^{3}(\boldsymbol{\varepsilon}_+^*)_i^+ + \sum_{i=1}^{3}(\boldsymbol{\varepsilon}_-^*)_i^+ \tag{10}$$

The independent damage parameters (D_T and D_C) are functions of the equivalent strain, ε_{d0} and a set of internal parameters (A_T, B_T, A_C, B_C,) calibrated to represent concrete behavior in tension and compression observed by uniaxial experimental tests as:

$$\begin{aligned} D_T &= 1 - \frac{\varepsilon_{d0}(1-A_T)}{\tilde{\varepsilon}} - \frac{A_T}{e^{B_T(\tilde{\varepsilon}-\varepsilon_{d0})}} \\ D_C &= 1 - \frac{\varepsilon_{d0}(1-A_C)}{\tilde{\varepsilon}} - \frac{A_C}{e^{B_C(\tilde{\varepsilon}-\varepsilon_{d0})}} \end{aligned} \tag{11}$$

Mazars (1984) proposed some limits for these internal parameters based on several experimental analyses as following:

$$\begin{aligned} 0{,}7 \leq A_T \leq 1{,}0 \\ 10^4 \leq B_T \leq 10^5 \end{aligned} \tag{12}$$

$$1{,}0 \leq A_C \leq 1{,}5$$

$$10^3 \leq B_C \leq 2 \times 10^3$$

Finally, the real stress tensor at the point assumes the form:

$$\boldsymbol{\sigma} = (1 - D)\mathbf{C}\colon \boldsymbol{\varepsilon} \tag{13}$$

It is worthy to mention that the (1 – D) penalizes all the stress components on the stress tensor, even the shear stress. Therefore, the isotropic behavior of the damage model still stands over the complete stress tensor.

2.3 Elastoplastic Model for Steel

Steel has as main feature, the presence of a plastic behavior after it reaches the yielding stress. It means that in case of an unloading process, at any stage of the analysis, a residual strain appears and cannot be recovered. Therefore, an elastoplastic behavior is observed, in which after yielding there are two possibilities: the perfect elastoplastic way and the elastoplastic with linear isotropic hardening way. In the first on, the normal stress keeps constant equal to the yielding stress until the physical breakage of steel. In the second one, a hardening phase emerges after yielding, in which some loss of stiffness is observed, but the material is still able to resist until the breakage. In the numerical modelling, the mathematical difference between the two approaches is in the plastic coefficient of steel (Ks). For perfect elastoplastic behavior, Ks = 0 and for the elastoplastic with linear hardening, Ks ≠ 0, varying from 1% to 10% of the steel Young modulus (Es). Figure 2 shows these two approaches for steel modelling adopted in this work. As the longitudinal and transversal reinforcement are defined by several layers along the cross section and the finite element length, respectively, an uniaxial plasticity approach was adopted. In such case, the main objective of the algorithm consists in to correct the elastic predictor stress, which is defined only by one value (σs) at the reinforcement layer.

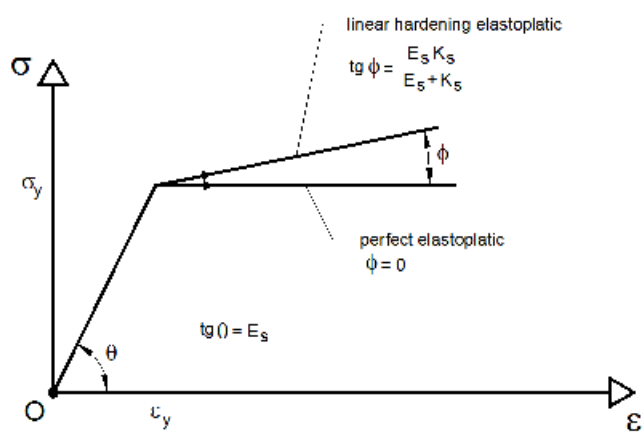


Figure 2: Elastoplastic behavior for steel.

The plasticity algorithm to the corrected stress assessment is described below and it is applied to each longitudinal reinforcement layer and stirrups along the element length. The nomenclature *i+1* stands for the actual increment and *i* corresponds to the last converged increment.

A) Evaluate the current strain (ε^{i+1}) by:

$$\varepsilon^{i+1} = \varepsilon^{i} + \Delta\varepsilon^{i+1} \tag{14}$$

B) Evaluate the current elastic predictor stress (σ^{i+1}) by:

$$\sigma^{i+1} = E_S\left(\varepsilon^{i+1} - \varepsilon_p^{i+1}\right) \tag{15}$$

C) Plastic criterion verification (f^{i+1}):

$$f^{i+1} = \sigma^{i+1} - \left(\sigma_Y + K_S\alpha^{i+1}\right) \leq 0 \tag{16}$$

The steel plasticizes if the condition $f^{i+1} > 0$ is achieved; on the other hand, the steel remains elastic. The next steps occur just in case of the plastic criterion is not verified, i.e., if $f^{i+1} > 0$.

D) Evaluate the current increment of the plastic strain ($\Delta\lambda$) by:

$$\Delta\lambda = \frac{E_S\Delta\varepsilon^{i+1}sign\left(\sigma^{i+1}\right)}{(E_S + K_S)} \tag{17}$$

The function *sign (.)* only takes into account the signal of the stress to differentiate tension and compression layers and assumes the form:

$$\begin{aligned} sign\left(\sigma^{i+1}\right) &= +1 \ \rightarrow for\ \sigma^{i+1} > 0 \\ sign\left(\sigma^{i+1}\right) &= -1 \ \rightarrow for\ \sigma^{i+1} < 0 \end{aligned} \tag{18}$$

E) Evaluate the current plastic strain (ε_p^{i+1}) by:

$$\varepsilon_p^{i+1} = \varepsilon_p^{i} + \Delta\lambda sign\left(\sigma^{i+1}\right) \tag{19}$$

F) Evaluate the current value for α^{i+1} by:

$$\alpha^{i+1} = \alpha^{i} + \Delta\lambda \tag{20}$$

G) Evaluate the corrected steel's Young modulus (E_S') by:

$$E_S' = \frac{E_S K_S}{(E_S + K_S)} \tag{21}$$

H) Evaluate the corrected stress (σ^{i+1}) by:

$$\sigma^{i+1} = E_S'\varepsilon^{i+1} \tag{22}$$

In which: ε^{i} is the strain at the last converged increment; $\Delta\varepsilon^{i+1}$ is the current strain increment; ε_p^{i+1} is the residual or plastic strain; σ_Y is the steel yielding stress; α^{i+1} and α^{i} corresponds to the total cumulated plastic strain at the current and the last converged increment, respectively; $\Delta\lambda$ is increment of the plastic strain.

Note that, the new value of α every time plastic strains increase means that the plastic surface size also increases.

If the plastic criterion is not violated, the current stress at the reinforcement remains the same assessed by the elastic predictor in Equation 15. It means that $\Delta\lambda = 0$ and there is no plastic strain yet or there is no evolution of the plasticization.

2.4 Shear Resistance Model with Stirrups

In standards approaches of unidimensional FEM, the transversal reinforcement contribution is not take into account. The finite element stiffness matrix is constructed considering the influence of the concrete and longitudinal reinforcement, but none reference is done about the stirrups. It happens because in both cases, concrete and reinforcement bars are subjected by normal stresses acting in X axis (longitudinal direction). But in case of the transversal reinforcement, although the stirrups branches are subjected too by normal stresses, these stresses act in the Y axis (transversal direction). In traditional beams, the transversal normal stress σ_y can be neglected and the stress state at any point has only two components: normal stress σ_x and shear stress γ_{xy}. Therefore, there is no direct connection between σ_y and the stress acting along the stirrups.

Belarbi and Hsu (1990) carried out experimental tests in T cross section RC beams to observe the stress distribution along vertical stirrups and to assess from what moment the stirrups really contribute to resist shear forces. They observed that the magnitude of the stresses increases from the compressed banzo to tensile banzo, but decreases near the longitudinal reinforcement. It is also observed that the real contribution of the transversal reinforcement occurs after the concrete cracking. Before this, only the undamaged concrete and the aggregate interlock for low values of damage support all the shear stresses. Based on this behavior, it was adopted here the alternative model proposed by Nogueira (2010), which considers the presence of the transversal reinforcement by its geometrical rate along the beam and its contribution only after the damage process begins. In this way, the shear reinforcement contribution is linked with the damage model sharing the same criterion to starts its effects. As the equivalent strain is defined by the sum of positive components of the strain tensor, damage is associated only to stretching (tension strains). Furthermore, it is considered that in concrete, the opening of diagonal cracks is directly associated to the main tension strain ε_1. Because of such behavior, it will be assumed that the stirrups strain will be also associated to ε_1, but only to the dissipated portion as described below.

After damage beginning, it is considered the split of the strain tensor in two parts: the elastic one (e index) which can be recovered and the damaged one (d index), which is dissipated during the process of damaging evolution.

$$\boldsymbol{\varepsilon} = \boldsymbol{\varepsilon}^{\mathbf{e}} + \boldsymbol{\varepsilon}^{\mathbf{d}} \tag{23}$$

In the same way, the real stress tensor at a point can be splitted in an elastic and damaged part as:

$$\boldsymbol{\sigma} = (1 - D)\mathbf{C}\colon\boldsymbol{\varepsilon} = \mathbf{C}\colon\boldsymbol{\varepsilon} - D\mathbf{C}\colon\boldsymbol{\varepsilon} \tag{24}$$

Concrete is responsible to resist the first term of the Equation 24. The second term given by $D\mathbf{C}:\boldsymbol{\varepsilon}$ can be rewritten as:

$$\boldsymbol{\sigma}^{d} = D\mathbf{C}:\boldsymbol{\varepsilon} = \mathbf{C}:\boldsymbol{\varepsilon}^{\mathbf{d}} \tag{25}$$

In which: $\boldsymbol{\varepsilon}^{\mathbf{d}}$ is the damaged strain tensor at a point due the evolution of the damage.

However, as the stirrups are subjected only to normal stresses, the transversal reinforcement strain will be given by the dissipated part of the main tension strain ε_1, defined by ε_1^{d}, rotated to the reinforcement direction, which is, in general, vertical. In the same way, the compressed strut in a point will have the same strain of the main compression strain ε_2. Those values are all assessed in each integration point along the cross section of the elements. Following the observations made by the Belarbi and Hsu (1990) tests, the stirrup's strain, as depicted in Figure 3, will be the maximum value of ε_1^{d} rotated to vertical direction along the cross section as:

$$\varepsilon_{sw} = \max[\varepsilon_1 D \sin\alpha] = \max\left[\varepsilon_1^{d} \sin\alpha\right] \tag{26}$$

In which: α is the main direction related to ε_1.

At the fibers nearby the tension longitudinal reinforcement, the stirrup's strain will be very low because the main direction for tension is almost zero, which means there will be no transversal component. On the other hand, at the compressed fibers nearby the longitudinal reinforcement, the values of the damage parameter D and the ε_1 are also very low and offer a tiny contribution for the transversal reinforcement. Therefore, the higher values of the rotated damaged strain will be addressed around the middle of the cross section, but not necessary at its center. This approach to assess the stirrup's strain considers the nonlinear behavior of the concrete.

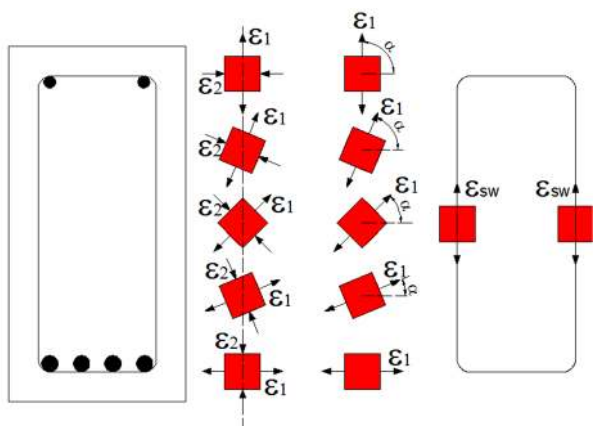


Figure 3: Distribution of the main tension strain along the cross section and the adopted stirrup's strain.

After the assessment of the stirrup's strain, the equivalent normal stress is given by the same elastoplastic model for steel described in the section 2.3. Figure 4 shows the truss analogy proposed by Ritter-Mörsch adopted to obtain the force transferred to the transversal reinforcement.

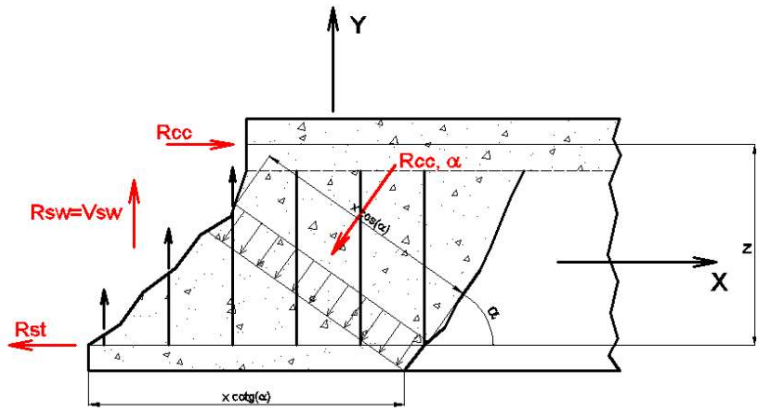


Figure 4: Force distribution for a cracked concrete element.

The forces R_{cc} and R_{st} are, respectively, the resultants on the compressed concrete zone and the longitudinal tension reinforcement. The model assumes that the force $R_{cc,\alpha}$ along the compressed strut is already taken into account by the concrete contribution in shear force. Thus, the force in the transversal reinforcement V_{sw} can be evaluated by the product between the reinforcement area A_{sw} and the stirrup stress σ_{sw} for each band equal to the effective depth d of the cross section as:

$$V_{sw} = \sigma_{sw}\rho_{sw}b_w d \tag{27}$$

In which: ρ_{sw} is the geometric transversal reinforcement rate and can be given by $A_{sw}/s_w b_w$; b_w corresponds to the cross section width of the element; s_w is the spacing between stirrups.

2.5 Kent and Park's Confinement Model for Concrete

The original formulation of the Kent and Park (1971) model for concrete in compression was adopted to simulate the confinement effect due to the transversal reinforcement. The model was first developed to be used in compressed elements, but it was already used to study the influence of confinement in RC beams in bending (Delalibera, 2002; Lee and Pan, 2003). The main purpose of this model is to increase ductility (but not resistance) by considering a soft linear post peak behavior of the compressed concrete, as depicted in Figure 5.

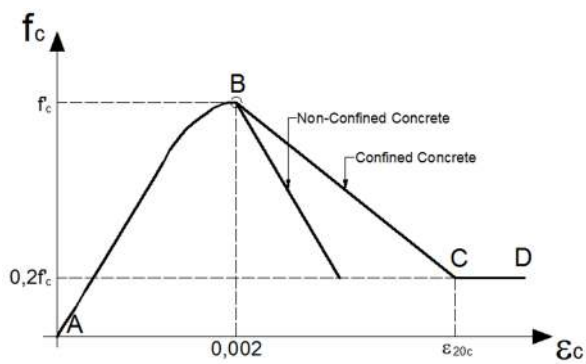


Figure 5: Kent and Park's constitutive law for concrete in compression.

The constitutive law is divided in three parts with the following equations to describe each part:

- AB: $\varepsilon_c \leq 0{,}002$

$$f_c = f_c' \left[\frac{2\varepsilon_c}{0{,}002} - \left(\frac{\varepsilon_c}{0{,}002} \right)^2 \right] \tag{28}$$

In which: f_c' is the compressive strength of non-confined concrete in MPa; f_c corresponds to the apparent compressive strength of the confined concrete in MPa; ε_c is the strain of the non-confined concrete.

- BC: $0{,}002 \leq \varepsilon_c \leq \varepsilon_{20c}$

$$f_c = f_c'[1 - z_c(\varepsilon_c - 0{,}002)] \tag{29}$$

In which: ε_{20c} corresponds to the strain of the confined concrete at $0{,}2f_c'$; z is the parameter that defines the slope of the descending branch of the curve and depends on the volumetric transversal reinforcement ratio. The parameter z assumes the form:

$$z_c = \frac{0{,}5}{\left(\frac{3 + 0{,}29 f'_c}{145 f_c - 1000} \right) + \left(\frac{3}{4} \rho_{vw} \sqrt{\frac{b_{vw}}{s_{vw}}} \right) - 0{,}002} \tag{30}$$

In which: ρ_{vw} is the volumetric transversal reinforcement ratio; b_{vw} is the width of the confinement zone at the cross section in millimeters; s_{vw} is the spacing between the stirrups used to confine the concrete in millimeters.

- CD: $\varepsilon_c \geq \varepsilon_{c20}$

$$f_c = 0{,}2 f'_c \tag{31}$$

In the CD branch, it is considered that the structural element has achieved the strain referent to 20% of the maximum concrete strength in tension.

It is worthy to mention that unconfined concrete can also be modeled with the described model by considering $\rho_{vw} = 0$ and deleting the response beyond C.

2.6 Calibration Technique for Internal Damage Parameters

The proposed ranges for the internal parameters of the Mazars' damage model are very large, especially in case of B_T and B_C. Furthermore, there are several combinations between these parameters that can give different structural responses to the analyzed RC system. In order to find the best set of parameters to simulate the desired structural behavior without a lot of trials and errors tests, a general approach was developed to calibrate the internal damage parameters. The main purpose of the calibration process is to minimize the relative error between the known and unknown answers in order to approximate the idealized structural response to the "real" one, as illustrated in Figure 6.

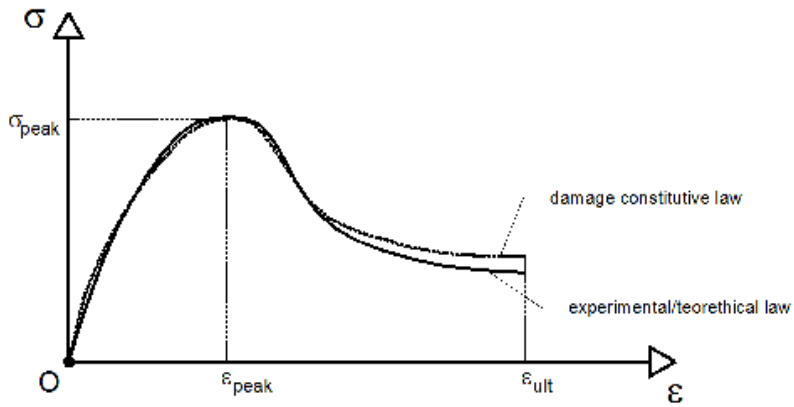


Figure 6: Comparison between idealized (damage constitutive law) and the "real" (experimental/theoretical) behavior.

To achieve this, the problem can be formulated by using the Least Square Method according to:

$$F(X,U) = \frac{1}{2}\sum_{i=1}^{n}[f_i(X,U)^2] \tag{32}$$

In which: U and X are, respectively, the parameters set that will not and that will be calibrated; n corresponds to the number of known answers from the experimental data or from the theoretical source; f is defined as the local error function and gives the differences between the known and the unknown answers of the experiment. In such case, the problem consists in represent the concrete behavior, in tension and compression, by the constitutive law proposed by the Mazars' damage model. In the absence of experimental data for several concrete classes of strength, with or without the presence of the confinement effect, theoretical laws in the literature can be used to give the responses in uniaxial tension (T) and compression (C) tests. Thus, the local error functions assume the form:

$$\begin{aligned} f_T(X_T,U) &= \sigma_{T,known} - [1 - D_T(X_T,U)]E\varepsilon_T \\ f_C(X_C,U) &= \sigma_{C,known} - [1 - D_C(X_C,U)]E\varepsilon_C \end{aligned} \tag{33}$$

In which: D_T and D_C are, respectively, the damage parameters for tension and compression given by Equation 11; E is the concrete Young modulus; ε_T and ε_C are, respectively, the concrete strain in the uniaxial test for tension and compression. In case of compression, $\sigma_{C,known}$ is assessed by Kent and Park's model described by Equations 28, 29 and 31. Regarding concrete behavior in tension, the $\sigma_{T,known}$ is given by the Figueiras' constitutive law (1983) or any other law.

The fitting of the parameters is performed through an iterative process starting from an initial trial $X_{C0} = (A_C, B_C)$ and $X_{T0} = (A_T, B_T)$ normally adopted as the medium values recommended by Mazars (Equation 12). For each iteration process, the vectors X_C and X_T are replaced by a new trial solution given by $(X_C + H_C)$ and $(X_T + H_T)$ until reach the convergence. The following formulation has to be applied to tension and compression independently, but to simplify the description of the development, the next steps will address a general way.

To formulate that, a function *F(X+H, U)* can be approximated by a Taylor's series expansion:

$$F(X+H,U) = F(X,U) + H^T(X)G(X,U) + \frac{1}{2}H^T(X)Q(X,U)H(X) \; or \; simplifying$$
$$F(X+H,U) = F + H^T G + \frac{1}{2}H^T QH \tag{34}$$

In which: G and Q are, respectively, the gradient and the hessian matrices of the function F; H indicates a descendant direction for F to the minimum point.

The gradient and hessian matrices assume the form:

$$G(X,U) = \begin{bmatrix} \partial F/\partial x_1 \\ \cdots \\ \cdots \\ \partial F/\partial x_k \end{bmatrix} \tag{35}$$

$$Q(X,U) = \begin{bmatrix} \partial^2 F/\partial x_1 x_1 & \cdots & \partial^2 F/\partial x_1 x_k \\ \vdots & \ddots & \vdots \\ \partial^2 F/\partial x_k x_1 & \cdots & \partial^2 F/\partial x_k x_k \end{bmatrix} \tag{36}$$

In which: k corresponds to the number of calibrated parameters (in such case k = 2).

In order to simplify the understanding but without loss of generality, the same minimization process can be written using the local error function *f*. Assuming that *f* and its derivatives are continuous in the considered domain, the gradient G and the hessian matrix Q can now be described as:

$$G(X,U) = \begin{bmatrix} \sum_{i=1}^{n} \frac{\partial f_i(X,U)}{\partial x_1} f_i(X,U) \\ \sum_{i=1}^{n} \frac{\partial f_i(X,U)}{\partial x_2} f_i(X,U) \end{bmatrix} \tag{37}$$

$$Q(X,U) = \begin{bmatrix} \sum_{i=1}^{n} \frac{\partial f_i(X,U)}{\partial x_1}\frac{\partial f_i(X,U)}{\partial x_1} + f_i(X,U)\frac{\partial^2 f_i(X,U)}{\partial x_1 \partial x_1} & \sum_{i=1}^{n} \frac{\partial f_i(X,U)}{\partial x_1}\frac{\partial f_i(X,U)}{\partial x_2} + f_i(X,U)\frac{\partial^2 f_i(X,U)}{\partial x_1 \partial x_2} \\ \sum_{i=1}^{n} \frac{\partial f_i(X,U)}{\partial x_2}\frac{\partial f_i(X,U)}{\partial x_1} + f_i(X,U)\frac{\partial^2 f_i(X,U)}{\partial x_2 \partial x_1} & \sum_{i=1}^{n} \frac{\partial f_i(X,U)}{\partial x_2}\frac{\partial f_i(X,U)}{\partial x_2} + f_i(X,U)\frac{\partial^2 f_i(X,U)}{\partial x_2 \partial x_2} \end{bmatrix} \tag{38}$$

In which: the $\frac{\partial f_i(X,U)}{\partial x_k}$ terms are the Jacobean (J) of the function and can be described as:

$$J(X,U) = \begin{bmatrix} \frac{\partial f_1(X,U)}{\partial x_1} & \frac{\partial f_1(X,U)}{\partial x_2} \\ \vdots & \vdots \\ \frac{\partial f_i(X,U)}{\partial x_1} & \frac{\partial f_i(X,U)}{\partial x_2} \end{bmatrix} \tag{39}$$

The Equations 37 and 38 can be rewritten in the contracted form as:

$$G(X,U) = J^T(X,U)f(X,U) \tag{40}$$

$$Q(X,U) = J^T(X,U)J(X,U) + \sum_{i=1}^{n} f_i(X,U)f_i''(X,U) \tag{41}$$

To solve the problem proposed by Equation 32, the Gauss-Newton technique was adopted. This approach uses a linear approximation to function *f(X,U)* at the neighborhood of point X, which allows, by an expansion in Taylor's series, write the value of the *f(X+H,U)* according to:

$$f(X+H,U) \cong f(X,U) + J(X,U)H \tag{42}$$

Replacing Equation 42 in 34, the lagrangean *L(H)* of the function *F* can be obtained as:

$$F(X+H,U) \cong L(H) \cong F(X,U) + H^T J^T(X,U)f(X,U) + \frac{1}{2}H^T J^T(X,U)J(X,U)H \tag{43}$$

Therefore, the solution of the problem consists in to find the descendant direction H that minimizes *L(H)*. The gradient and the hessian considering now the lagrangean are given, respectively, by *L'(H)* and *L''(H)* as:

$$L'(H) = J^T(X,U)f(X,U) + J^T(X,U)J(X,U)H \tag{44}$$

$$L''(H) = J^T(X,U)J(X,U) \tag{45}$$

When H is close to zero, L'(H) = F'(H) and the condition of F'(H) = 0 can be replaced by L'(H) = 0. If the columns of the Jacobean matrix are linear independent, than the hessian of the lagrangean L''(H) is positive-definite, which guarantee that L(H) has a minimum point given by:

$$L'(H) = 0 \rightarrow J^T(X,U)f(X,U) + J^T(X,U)J(X,U)H = 0 \tag{46}$$

Finally, the vector H can be assessed by the solution of system:

$$L''(H)H = -[J^T(X,U)f(X,U)] \tag{47}$$

This an iterative procedure in which at the end of the m-iteration, the vector H is added to the last updated X. This procedure is repeated until the new H is the same as the one obtained at the last iteration. At the end of the calibration process, X_C and X_T provide the values of the internal damage model (A_C, B_C) and (A_T, B_T), respectively.

2.7 Solution of the Nonlinear Problem

In order to assess the ductility behavior of RC beams, an arc length displacement control technique was adopted. Because of the nonlinear nature of the problem, an incremental-iterative procedure coupled to the Newton-Raphson's technique to solve linear systems was used, in which the total displacement was applied in equal increments until the final displacement. For each increment, the necessary loading conditions were assessed according to the nonlinear material laws (damage for concrete and plasticity for steel). Furthermore, as the confinement effect is a function of the transversal reinforcement of the elements, the approximate model to compute the stirrups contribution

was also added to the nonlinear problem. As described by Equation 27, the contribution of the shear reinforcement was only considered for the internal forces assessment, which means that there was no addition of the stirrups contribution on the local stiffness matrix of the elements and, consequently, on the global stiffness matrix of the total system. Therefore, a consistent tangent matrix approach was not able to be used and a similar technique was adopted. The stiffness matrix was constructed at the beginning of each iteration, as in the tangent approach, but only considering the contributions of concrete and longitudinal steel. After the evaluation of the damage parameter for each integration point along the cross section height, the influence of the degradation state is taking into account to evaluate the contribution of such integration point at the assessment of the local stiffness matrix for the next iteration. More details about the FEM mechanical model can be found in Nogueira et al. (2013).

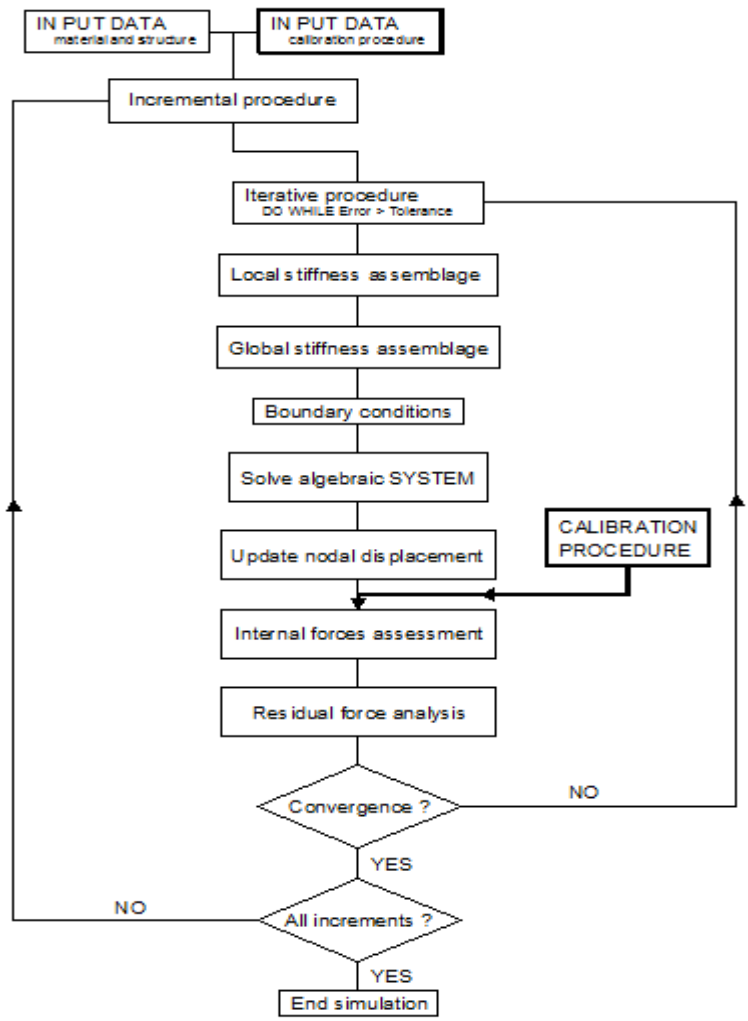


Figure 7: Flowchart of the mechanical model including the calibration procedure.

Figure 7 shows a schematic flowchart of the mechanical model with the introduction of the parameters calibration procedure. Some details about the main steps are discussed below.

– IN PUT DATA (material and structure/calibration procedure): the elastic material properties, loading/displacement parameters and structure information are all described here. Regarding the calibration procedure, the first trials for the tension and compression parameters of the damage model are given: $X_{C0} = (A_C, B_C)$ and $X_{T0} = (A_T, B_T)$. The limit value of the strain for each tension and compression is also given for the discretization process to approximate the theoretical constitutive law. The number of strain increments is another parameter and it is represented by the n value in Equation 32;
– Local stiffness assemblage: the local stiffness matrix of each finite element $[k]_{FE}$ is given by:

$$[k]_{FE} = [k]_{c,flexure} + [k]_{c,shear} + [k]_{s,longitudinal} \tag{48}$$

In which: $[k]_{c,\ flexure}$ is the contribution of concrete in flexure (bending moment); $[k]_{c,\ shear}$ is the contribution of concrete in shear; $[k]_{s,\ longitudinal}$ is the contribution of longitudinal reinforcement. It is worth to mention that the contribution of the shear reinforcement (stirrups) is not considered.

– Global stiffness assemblage: the global stiffness matrix is constructed here by the sum of each element stiffness matrix;
– Internal forces assessment: in this subroutine of the mechanical model, the internal efforts normal force, shear force and bending moment for each finite element node are evaluated considering the updating of damage and plastic strains that may occur along the loading process. But before such calculations, for each finite element, the damage parameters are calibrated according to the described procedure in section 2.6. It is evident that if there are no different concrete strengths along the finite element mesh, this procedure can be done only once at the beginning of the internal forces assessment subroutine and keeps constant for all the subsequent steps of the simulation.

With this approach of incremental displacement applied, it is possible to represent the post peak softening branch of the structural behavior of the beams and evaluate the ductility.

3 DUCTILITY OF REINFORCED CONCRETE ELEMENTS

The approach to assess the curvature ductility or also called as ductility factor adopted in this work is based on the one described by Lee and Pan (2003). Hence, the ductility factor (μ_ϕ) can be given by:

$$\mu_\phi = \frac{\phi_u}{\phi_y} \tag{49}$$

In which: ϕ_u is the ultimate curvature of the analysed cross section; ϕ_y is the yielding curvature at the same cross section.

The yielding curvature is defined when the longitudinal reinforcement reaches the steel yielding stress, while the ultimate curvature must be carefully adopted. Ductility may be defined as the ability of the element to deform without significant loss of resistance. Based on this definition, many researchers have adopted for ultimate curvature their own interpretation for the phenomenon. Ziara et al. (1995), supported by investigations of flexure behavior in reinforced concrete beams,

defined the ultimate curvature when the compressed strain of the concrete compressed fiber at the same layer of compressed reinforcement reached the value of 5,0‰. Eurocode 8 and Lopes et al. (2012) considered that ultimate curvature is defined by the correspondent curvature at 85% of the resistant cross section bending moment, after the peak of the equilibrium trajectory has be achieved. In this paper, the ultimate curvature was obtained from the correspondent value of ultimate bending moment at the analyzed cross section given by the ultimate load of the whole structure. Figure 8 illustrates the adopted approach. The marks Y and U stand for yielding curvature and ultimate curvature, respectively, while the $0{,}85P_{max}$ indicates de ultimate curvature considered by Lopes et al. (2012). As a displacement control process over the structure was applied, when the ultimate load is reached, the correspondent curvature at the considered cross section is adopted as the ultimate curvature. In such way, the ultimate curvature does not depend on a specific value of strain in any position of the cross section, which grants to this approach a general aspect. Furthermore, the ultimate curvature reflects, at the studied cross section, the global resistance of the considered structural element.

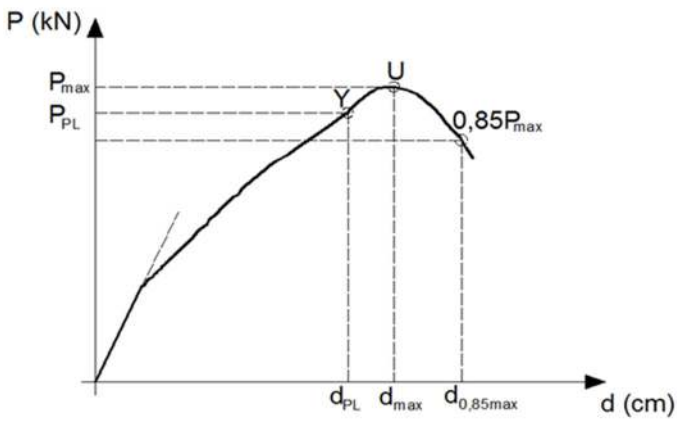


Figure 8: Yielding and ultimate curvature adopted in the study.

4 PARAMETRIC ANALYSIS

To perform the assessment of the ductility factor in reinforced concrete beams, a parametric analysis was carried out. The numerical analyses were conducted in order to show the influence of the confinement effect provided by different transversal reinforcement rates over the ductility of the RC beams at the ultimate limit state. Moreover, another question motivated the numerical tests, which was: is there any compromise between longitudinal and transversal reinforcement that influences the ductile behavior of RC beams? To answer these questions the following steps were performed and they are described below.

The parametric analysis was carried out considering three classes of concrete strength (f_{ck}): 20, 30 and 40 MPa, which were indicated by C20, C30 and C40 respectively. For each concrete class, four different values of relative neutral axis position (β_x) were adopted to design the RC beams against bending moment. With this, four different values of cross sections heights and longitudinal reinforcement rates were obtained. According to many standard codes for RC elements design (such

as ABNT NBR 6118, EUROCODE 2 and others), a limitation of the neutral axis position must be imposed to guarantee the ductile behavior of the elements. For example, the Brazilian code (ABNT NBR 6118) defines such limit for β_x, as 0,450 in case of concretes with characteristic compression strength until 50MPa. Beyond this value, the ductility is impaired and a brittle behavior produced by the concrete crushing may occur, which must be avoided in practice. Then, for each value of β_x, another four situations were considered regarding the amount of transversal reinforcement to assess the influence of the confinement effect over ductility. The cases "*without conf.*" and "*design 0*" have the same volumetric transversal reinforcement rate, but in the first one, there is no confinement effect and in the second one, this effect was taking into account by the Kent and Park's constitutive law. "*Designs 1*" and "*2*" were adopted decreasing the spacing between consecutive stirrups taking as reference those values achieved in "*design 0*", by 60% and 30%, respectively. Figure 9 summarizes all the adopted models tested in the parametric analysis. The legend xx indicates 20, 30 and 40 MPa. Therefore, $16 \times 3 = 48$ numerical analyses were performed in the ductility study. The results are shown in the section 5.2 of this article.

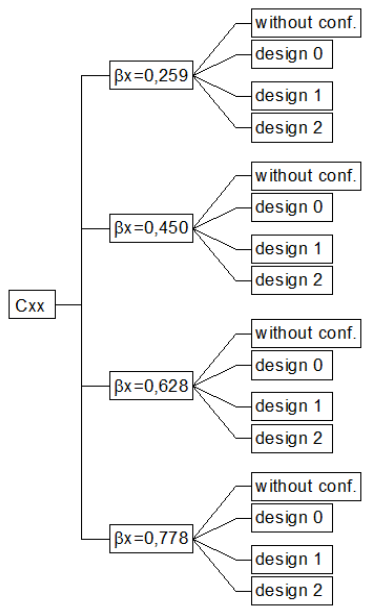


Figure 9: Flowchart of the parametric analysis for the ductility study.

The mechanical model based on MEF unidimensional approach coupled to all the described nonlinear models for concrete, steel and shear reinforcement were used in the parametric analyses.

5 RESULTS

5.1 RC beams Tested by Ziara et al. (1995)

Ziara et al. (1995) carried out experimental tests in reinforced concrete beams to simulate the confinement effect provided by shear reinforcement in their mechanical behaviour. The same beams

were numerically analysed by Delalibera (2002) and also with the proposed model described in this paper with the same purpose. The confinement effect was simulated by the calibration of the damage internal parameters considering the post peak stress-strain curve for concrete in compression according to Kent and Park's model. The beams are over reinforced and the stirrups were used all around the cross section, discounting only the concrete cover. Figure 10 shows the static scheme and the details of the analysed beam. Table 1 presents the material properties and other adopted parameters.

It was adopted for concrete: Poisson's ratio of 0,2 and transversal elasticity modulus G_c equals to $E_c/2{,}4$. For the steel, it was used a perfect elastoplastic behaviour model. The beams were analysed considering a regular finite elements mesh. For C2 beam, it was adopted 40 elements, in which: 5 elements for each 40 cm, 5 elements for each 37,5 cm and 10 elements on the central span of 130 cm. For C3.2 beam, it was adopted 46 elements, in which: 5 elements for each 37,5 cm, 8 elements for each 60 cm and 10 elements on the central span of 110 cm.

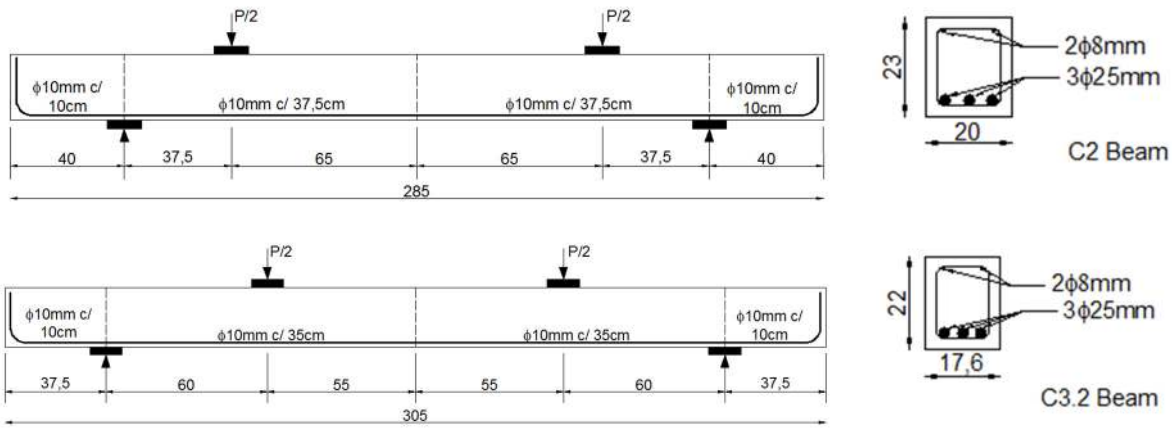


Figure 10: Beams tested by Ziara et a. (1995).

Beam	f_{ck} (MPa)	f_{tk} (MPa)	E_c (GPa)	f_{yk} (MPa)	f_{ywk} (MPa)	E_s (GPa)
C2	30,5	2,05	31	442	442	210
C3.2	19,6	1,53	25	442	442	210

Table 1: Material properties of the beams.

The beams modelling was carried out considering the Timoshenko theory (shearing deformation was taking into account), with the simplified model of shear reinforcement contribution. Concrete behaviour was simulated by the Mazars' damage model coupled with the automatic calibration process. The compression parameters of the model were calibrated according to Kent and Park's law (1971) with/without confinement and the tension parameters were calibrated according to Figueiras's law (1983). Table 2 shows the damage calibrated parameters for each beam and the minimum values proposed by Mazars used to compare the mechanical answer in both beams. The

ε_{d0} parameter, given by f_{tk}/E_c, is the specific deformation corresponding to the tensile strength of concrete. Therefore, to the group of minimum parameters, ε_{d0} assume the same values of the ones presented in Table 2 for C2 and C3.2 beam. The numerical integration was carried out with 6 points of Gauss along the length (PGL) and 20 points of Gauss along the height (PGH) of the finite elements. The loading process was performed with 0,025 cm vertical displacement increments in the central point (middle span).

Beam	ε_{d0}	A_T	A_C	B_T	B_C
C2 with confinement	$6{,}61\times10^{-5}$	0,722	0,863	10987,134	1213,796
C2 without confinement	$6{,}61\times10^{-5}$	0,722	1,788	10987,134	2455,530
C3.2 with confinement	$6{,}12\times10^{-5}$	0,718	0,631	11617,602	1194,646
C3.2 without confinement	$6{,}12\times10^{-5}$	0,718	0,937	11617,602	1902,636
Minimum	-------	0,7	1,0	10000,0	1000,0

Table 2: Internal parameters of the damage model.

Figure 11 shows the numerical equilibrium path of the C2 and C3.2 beams compared to the experimental and numerical responses obtained by Ziara et al. (1995) and Delalibera (2002), respectively. The mechanical model used by Delalibera (2002) was based on MEF with a plane frame finite element of 2 conventional nodes (one in each element's edge) and 3 degrees of freedom per node (two translations and one rotation). Concrete was represented, in tension and compression, by the constitutive laws of CEB-FIP (1991), while steel was also simulated with elastoplastic behaviour. For the confined concrete, Delalibera (2002) adopted the model proposed by Saatcioglu and Razvi (1992), which changes the uniaxial behaviour of concrete on the confined zone by the stirrups.

Three set of damage parameters were used to simulate these beams with the proposed mechanical model: minimum, with and without confinement.

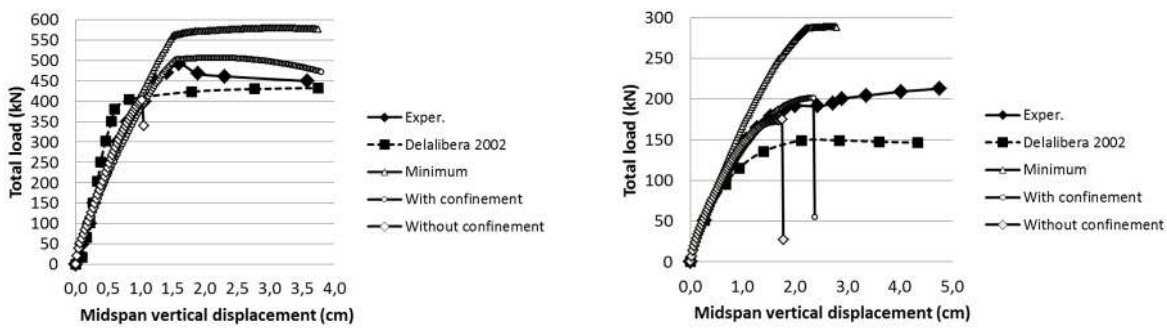


Figure 11: Equilibrium path for C2 and C3.2 beams.

Table 3 shows the ultimate load values obtained in the experimental tests and in all numerical modelling, as well as the differences between each model according to the experimental result given by the bias factor.

Beam	Ultimate load values (kN) / Bias factor ($P_{u,num}/P_{u,exp}$)				
	Experimental	Delalibera (2002)	Minimum	With confinement	Without confinement
C2	489,3	446,6 /0,91	578,9 / 1,18	506,2 / 1,03	403,2 / 0,82
C3.2	216,1	149,5 / 0,69	288,6 / 1,36	200,9 / 0,93	175,2 / 0,83

Table 3: Ultimate load and bias factor values.

The results show the sensitivity of the mechanical responses when the internal damage parameters are modified. The set of minimum parameters proposed by Mazars (1984) as one can see, on both beams, was not able to adequate represent the equilibrium path of the beams, resulting in high ultimate load values. In both beams, the developed mechanical model represented with good agreement the most part of the experimental response, especially in the case when confinement was taking into account, even when the confinement effect created by stirrup reinforcements was indirectly considered through the calibration of the damage parameters. In the response without confinement, after the most compressed concrete fibres reached the compressive strength, it was observed a quickly decrease in compression stress even for small values of strain. It means that the confinement can provide more ductility associated with some resistance for concrete in compression after peak.

In the C2 beam, the ultimate load assessed by the mechanical model with confinement was almost equal to the experimental value. After the peak, the model still was able to represent the softening branch of the equilibrium path. However, in the C3.2 beam, the ultimate load was also well represented, but a more brittle failure was observed with the numerical approach. The high value of longitudinal reinforcement rate associated with the low value of concrete strength (19,6 MPa) resulted, with the used damage model, in a numerical brittle failure behaviour.

5.2 Ductility Study

In this example, an isostatic simply supported reinforced concrete beam subjected to a vertical load at midspan was analyzed to quantify the ductility in ultimate limit state for different designs. Figure 12 shows the geometry of the beam and the finite element mesh adopted in the analyses. It was adopted 40 1D finite elements with the same length. For the nonlinear process of solution, the numerical integration was carried out with 6 PGL and 20 PGH for each finite element. The loading process was performed with 0,025 cm vertical displacement increments in the central point (middle span). In all cases, the RC beams were designed considering $P_k = 30$ kN.

The parametric analysis was carried out considering three classes of concrete strength (C20, C30 e C40), four relative neutral axis positions (β_x = 0,259; 0,450; 0,628; 0,778) and four transversal reinforcement configurations. The main purpose was to quantify the influence of the confinement effect produced by the stirrups arrangements on the beam ductility. The confinement effect was took into account from the calibration of the Mazars' damage parameters considering the constitutive law for compressive concrete proposed by Kent and Park (1971). According to such law, the confinement level depends on the volumetric ratio of transversal reinforcement of the beam.

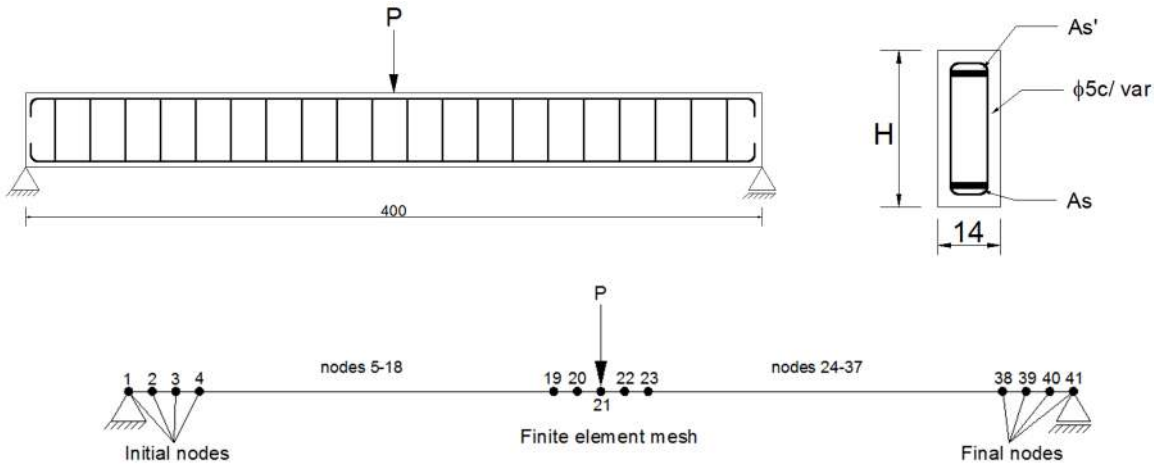


Figure 12: RC beam analyzed for the ductility study: dimensions in centimeters.

f_{ck} (MPa)	β_x	H (cm)	A_s (cm^2)	Without shear reinforcement	Design 0	Design 1	Design 2
20	0,259	40	2,95	$A_{sw} = 0$	ϕ5mm c/20cm: 1,96 cm^2/m	ϕ5mm c/12cm: 3,27 cm^2/m	ϕ5mm c/6cm: 6,54 cm^2/m
	0,450	33	4,07	$A_{sw} = 0$	ϕ5mm c/17cm: 2,31 cm^2/m	ϕ5mm c/10cm: 3,74 cm^2/m	ϕ5mm c/5cm: 7,14 cm^2/m
	0,628	30	5,03	$A_{sw} = 0$	ϕ 5mm c/15cm: 2,61 cm^2/m	ϕ5mm c/9cm: 4,36 cm^2/m	ϕ5mm c/4,5cm: 8,73 cm^2/m
	0,778	28	5,84	$A_{sw} = 0$	ϕ 5mm c/14cm: 2,81 cm^2/m	ϕ5mm c/8,5cm: 4,62 cm^2/m	ϕ5mm c/4cm: 9,82 cm^2/m
30	0,259	34	3,62	$A_{sw} = 0$	ϕ5mm c/18cm: 2,18 cm^2/m	ϕ5mm c/10,5cm: 3,74 cm^2/m	ϕ5mm c/5,5cm: 7,14 cm^2/m
	0,450	28	4,99	$A_{sw} = 0$	ϕ5mm c/14cm: 2,81 cm^2/m	ϕ5mm c/8,5cm: 4,62 cm^2/m	ϕ5mm c/4cm: 9,82 cm^2/m
	0,628	25	6,17	$A_{sw} = 0$	ϕ5mm c/12cm: 3,27 cm^2/m	ϕ5mm c/7cm: 5,61 cm^2/m	ϕ5mm c/3,5cm: 11,22 cm^2/m
	0,778	24	7,16	$A_{sw} = 0$	ϕ5mm c/11cm: 3,57 cm^2/m	ϕ5mm c/6,5cm: 6,04 cm^2/m	ϕ5mm c/3,5cm: 11,22 cm^2/m
40	0,259	30	4,18	$A_{sw} = 0$	ϕ5mm c/15cm: 2,62 cm^2/m	ϕ5mm c/9cm: 4,36 cm^2/m	ϕ5mm c/4,5cm: 8,73 cm^2/m
	0,450	24	5,76	$A_{sw} = 0$	ϕ5mm c/12cm: 3,27 cm^2/m	ϕ5mm c/7cm: 5,61 cm^2/m	ϕ5mm c/3,5cm: 11,22 cm^2/m
	0,628	22	7,12	$A_{sw} = 0$	ϕ5mm c/10cm: 3,93 cm^2/m	ϕ5mm c/6cm: 6,54 cm^2/m	ϕ5mm c/3cm: 13,09 cm^2/m
	0,778	21	8,26	$A_{sw} = 0$	ϕ5mm c/10cm: 3,93 cm^2/m	ϕ5mm c/6mm: 6,54 cm^2/m	ϕ5mm c/3cm: 13,09 cm^2/m

Table 4: Adopted values for the parametric study.

To illustrate all the designs considered for RC beam, Table 4 shows the total cross section height (H), relative neutral axis position (β_x), longitudinal reinforcement area (A_s) and the transver-

sal reinforcement (A_{sw}) for each resistance concrete class (f_{ck}). The RC beams were designed to shear forces using the model II of the ABNT NBR 6118 (2014), considering the inclination of 30º with horizontal for the compression struts. Thereafter, design 0 was obtained adopting the maximum value of distance between stirrups allowed by the Brazilian standard, while designs 1 and 2 were defined considering 60% and 30% of that maximum distance between stirrups, respectively.

Table 5 shows the mechanical properties of concrete used in the analyses. For the steel, in all case it was adopted yielding stress of 435 MPa, longitudinal elasticity modulus of 210 GPa and perfect elastoplastic behaviour.

f_{ck} (MPa)	f_{ctk} (MPa)	E_c (MPa)	Poisson	G_c (MPa)
20	1,55	25040	0,20	10435
30	2,03	30670	0,20	12780
40	2,45	35417	0,20	14757

Table 5: Concrete properties.

The Mazars' damage parameters (A_C, B_C, A_T, B_T) for concrete were obtained by calibration process, considering the constitutive laws of Kent and Park (1971) and Figueiras (1983) for compression and tension, respectively. Because of the calibration, the confinement effect was represented by the damage model according to the transversal reinforcement volumetric ratio. To illustrate some values, Table 6 presents the damage parameters obtained for each transversal reinforcement design considering all the concrete resistance classes, only for the design with $\beta_x = 0{,}259$. For the other values of the neutral axis relative position, the same method was applied to get the damage parameters. In the "Without shear reinforcement" case there is no confinement effect in the compressed concrete.

f_{ck} (MPa)	Stirrups	A_C	B_C	A_T	B_T
20	Without shear reinforcement	0,973	1923,668	0,720	11562,811
	Design 0	0,839	1661,882	0,720	11562,811
	Design 1	0,775	1520,801	0,720	11562,811
	Design 2	0,704	1348,268	0,720	11562,811
30	Without shear reinforcement	1,747	2431,449	0,723	11026,252
	Design 0	1,178	1775,246	0,723	11026,252
	Design 1	1,028	1537,857	0,723	11026,252
	Design 2	0,923	1347,658	0,723	11026,252
40	Without shear reinforcement	2,809	2836,434	0,726	10684,905
	Design 0	1,391	1732,878	0,726	10684,905
	Design 1	1,210	1492,230	0,726	10684,905
	Design 2	1,092	1314,011	0,726	10684,905

Table 6: Calibrated damage parameters for $\beta_x = 0{,}259$.

Figure 13 shows the bending moment × curvature relationship at midspan cross section for C20 with all the possibilities of neutral axis position and shear reinforcement design. As one can see, the lower neutral axis position, the higher is the horizontal plateau defined by the longitudinal rein-

forcement yielding. It indicates a ductile behaviour only by changing the amount of longitudinal reinforcement according to the neutral axis position, which stands for the ductility mentioned in the standard codes (comparison between the black curves). However, it was verified that is possible to increase the ductility on the ultimate limit state by making some changes in the stirrups design. In such cases, a bigger extension of the yielding plateau was achieved when the transversal reinforcement volumetric ratio was also increased, by closing the stirrups each other. The green curves indicate the higher value of the ductility compared to those in black ones for the same neutral axis position. Even for $\beta_x = 0{,}778$ it was observed a significant increase in the ductility of the beam. The same behaviour was achieved for the other values of the β_x. But, it is worthy to mention that the decreasing of the stirrups spacing provided much more ductility for lower values of the neutral axis position, which can be seen by the large extensions of the yielding plateau. In general, for C30 and C40 concrete resistance classes, the same behaviour was observed concerning the ductility as a function of β_x and amount of transversal reinforcement.

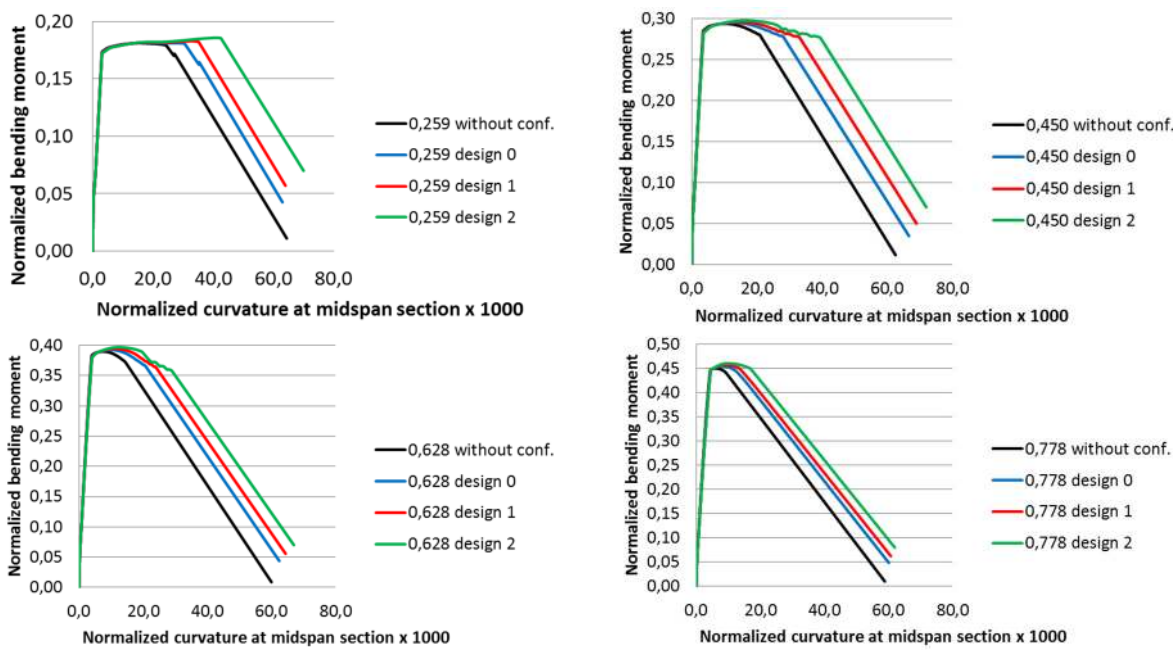


Figure 13: Bending moment × curvature relationship at midspan cross section: different shear reinforcement.

The results description can be completed by Figure 14, in which is showed the bending moment × curvature relationship for different neutral axis positions fixing each amount of transversal reinforcement (design) for C20. As noted, the combination of the two actions: decreasing of the relative neutral axis position and increasing of the volumetric transversal reinforcement ratio provided, in all the studied cases, a significant increase on the ductility of the beam.

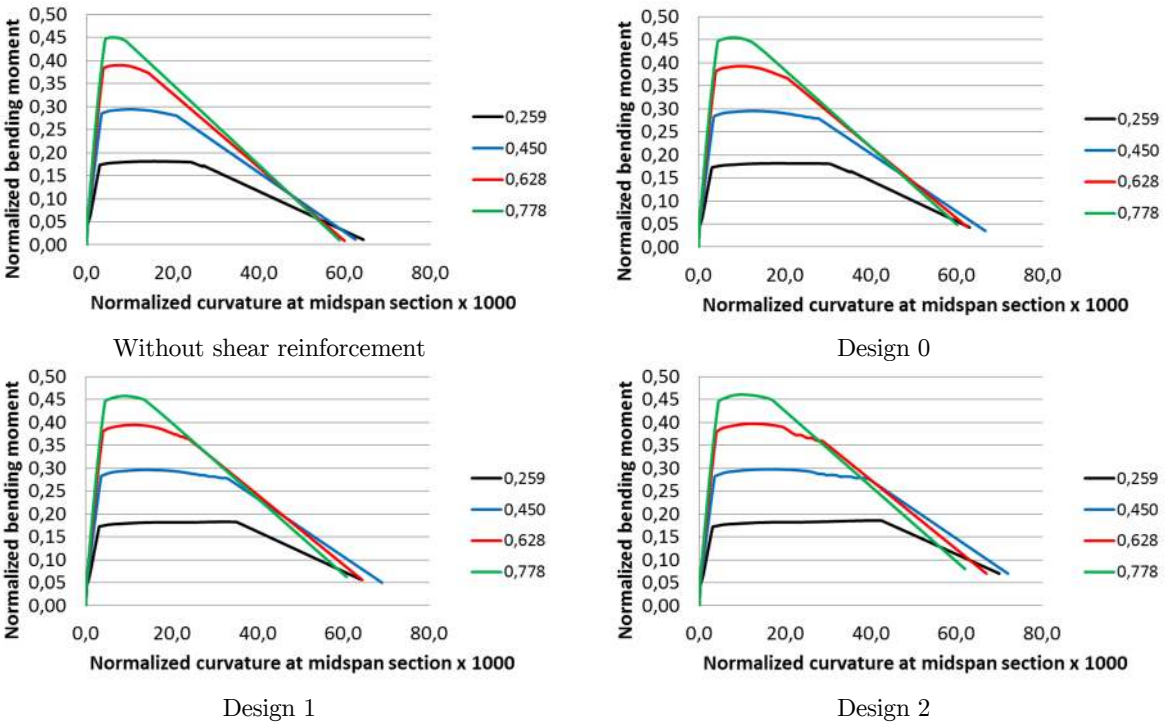
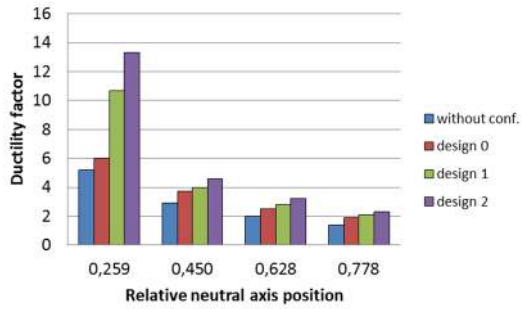


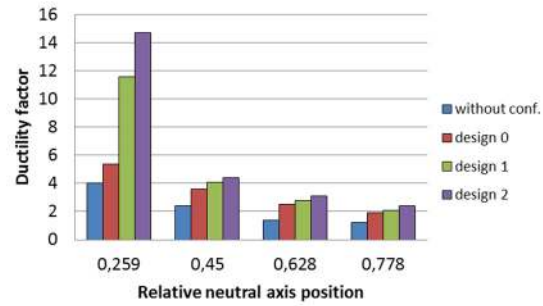
Figure 14: Bending moment × curvature relationship at midspan cross section: different neutral axis position.

The Figure 15 shows the assessed values of the ductility factor for all combinations of the neutral axis position and transversal reinforcement considering the confinement effect for each concrete resistance class. In all the analyzed cases, the confinement effect provided by the stirrups and their different designs increased the ductility of the RC beams. When the spacing between stirrups decreases, the confinement of the compressed zone in concrete increases, making that the compressive stress at the post-peak also increases compared to the same values without the effect of the confinement. In such cases, the RC beams can support more loading before the rupture is reached, which means an improvement on the ductility.

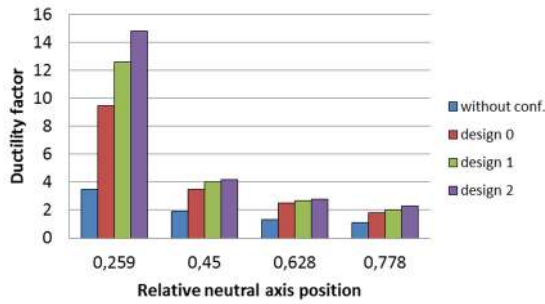
Another aspect that deserves to be discussed is the high efficiency of the stirrups design, in addition with the low values of the neutral axis position. As one can see in Figure 15, for lower values of β_x, such as 0,259, the influence of the confinement was expressive compared to the performance without this effect for all concrete resistance classes. The high capacity to deform before failure for beams designed with low values of the neutral axis position associated with high values of the volumetric transversal reinforcement rate, improved even more the ductility of the analysed RC beams. For example, for $\beta_x = 0{,}259$ and C20, the ductility factor varied from 5,2 (without confinement) to 13,3 (design 2), which means an increase of 155%. Considering the same case of β_x, but now for C30 and C40, the ductility factor varied from 4,0 to 14,7 and from 3,5 to 14,8 respectively, representing an increase of 267% and 322%. On the other hand, for $\beta_x = 0{,}778$, the improvement on ductility for C20, C30 and C40 were, respectively: 1,4 to 2,4 (increase of 64%); 1,2 to 2,4 (increase of 100%); 1,1 to 2,3 (increase of 109%).



C20



C30

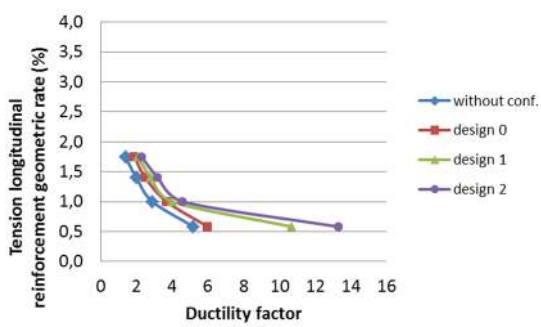


C40

Figure 15: Evolution of the ductility for each concrete resistance class.

Finally, the last aspect to be commented is the influence of the confinement over the different resistance classes of the concrete. The confinement effect, provided by the large values of the transversal reinforcement, was more significant in the beams belonged to C40 class than those belonged to C20 for the same relative neutral axis position. It means that in cases of concretes with high resistance, the transversal reinforcement design can be more effective than the neutral axis position when ductility is desired.

Figures 16 to 18 illustrate the relationship between the reinforcement rates and ductility factor for all concrete resistance classes.



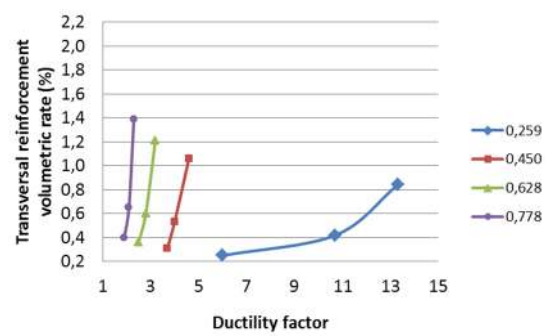


Figure 16: Longitudinal and transversal reinforcement rates × ductility factor: C20

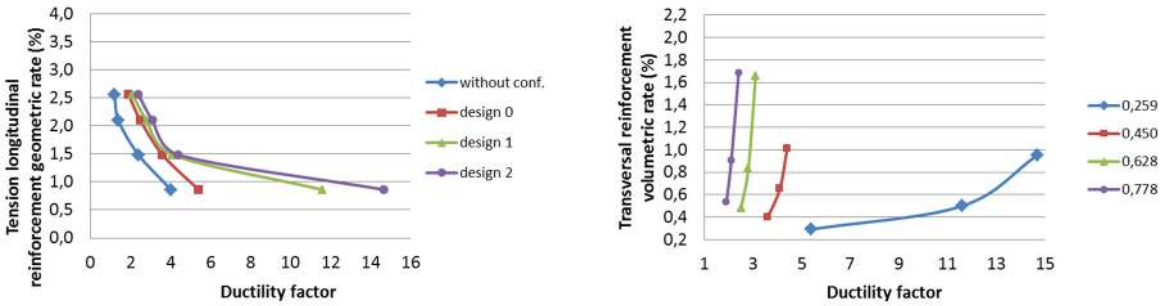


Figure 17: Longitudinal and transversal reinforcement rates × ductility factor: C30

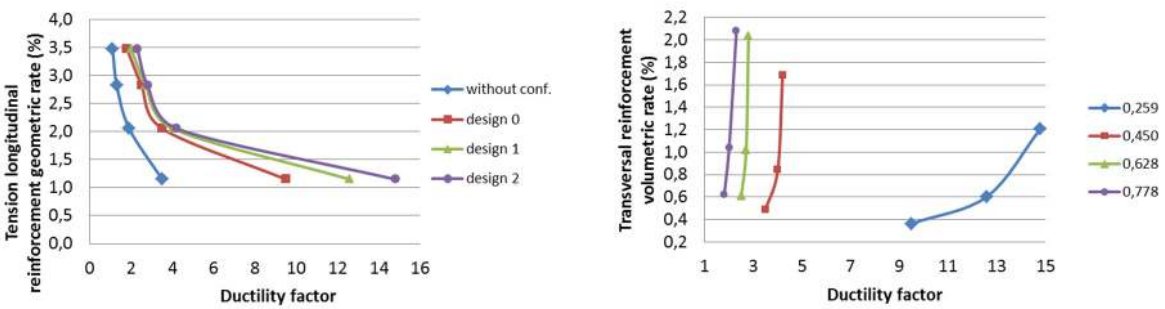


Figure 18: Longitudinal and transversal reinforcement rates × ductility factor: C40.

Regarding to the tension longitudinal reinforcement, the ductility factor increases as amount of reinforcement decreases. Therefore, ductile behaviors are achieved with low values of neutral axis position. When the confinement effect is taking into account, the same behavior is observed, but the ductility is significantly improved in such cases, especially for high resistance concretes (C40).

On the other hand, because of the confinement effect, the ductility factor increases as amount of transversal reinforcement also increases. At least for the analyzed cases, it was observed that the inclination of the curves regarding the horizontal axis shows the influence of the volumetric transversal reinforcement rate over the ductility of the beams. Note that such influence also depends on the neutral axis position. Thus, high values of transversal reinforcement in addition with low values of neutral axis position provide the better combination for the ductility at the ultimate limit state.

6 CONCLUSIONS

In this paper, an already developed mechanical model based on MEF unidimensional was coupled to some improvements in order to analyze ductility in reinforced concrete beams when the confinement effect is taking into account. The basis and all the details concerning to the finite element formulation and the nonlinear solution strategies of the problem, as described above, were developed and published in Nogueira et al. (2013), as some numerical examples to validate the model. To improve the capability of the model in simulate confinement effect, it was incorporate a module to calibrate the internal damage parameters set of the concrete, based on a specific constitutive law for concrete

in compression able to consider such effect. The Kent and Park's law was adopted in which the confinement effect is described depending on the volumetric transversal reinforcement rate at the post peak portion of the stress × strain relationship. Therefore, this module was implemented to the existent model coherently with the shear resistance model already working in the program. After that, the analyses were carried out for a generic isostatic RC beam to study the effect of the confinement on the ductility behavior of the beam. Some important points observed along the tests will be following discuss:

- The coupling of the existing mechanical model and the new module for calibration of the damage parameters worked very well and showed complete stability along the nonlinear solution process. When the beams tested by Ziara et al. (1995) were analyzed, the calibrated set of parameters were able to better represent the equilibrium trajectory of the beam than the minimum set proposed by Mazars (1984). Therefore, the results emphasize the importance of a proper definition of the damage parameters to simulate RC elements. With the developed calibration process and the knowledge of the constitutive law capable of to incorporate a desired effect, the numerical procedure can be applied to study the overall structure behavior;
- The influence of the longitudinal reinforcement on ductility is defined by the relative neutral axis position along the cross section of the element. For lower values of neutral axis position, the RC beams have higher cross section heights and, consequently, lower longitudinal reinforcement rates, which grant more ductility to these beams at the ultimate limit state. When the concrete resistance increases, the amount of longitudinal reinforcement required to maintain the same ductility also increases. Therefore, it was observed a direct dependence between the ductility factor and the longitudinal reinforcement rate;
- Regarding the transversal reinforcement, the confinement effect on the compressed zone of the cross section provided by this kind of reinforcement influences significantly the ductility. As the volumetric transversal reinforcement rate increases, the confinement effect also increases providing an extension of the ductile plateau, which means an improvement of the ductility factor. So, answering the proposed question written in section 4 of this paper: yes, there is an interaction between longitudinal and transversal reinforcement that influences ductility. High values of shear reinforcement coupled to low values of longitudinal reinforcement give the better combination for ductility. However, more tests must be carried out, especially the experimental ones to complete finish the research.

Acknowledgements

To FAPESP process 2016/14450-6 for the financial support of this project and to State University of São Paulo – UNESP.

References

ABNT NBR 6118 (2014). Design of concrete structures: procedure, Rio de Janeiro, Brazil.

ACI Committee 318 (2002). Buildings code requirements for structural concrete, Farmington Hills, Michigan – American Concrete Institute.

Araújo, J.M., (2009). Design of reinforced concrete cross sections subjected to flexure with emphasis in the ductility, Teoria e Prática na Engenharia Civil 14: 1-13.

Arslan, M.K., (2012). Estimation of curvature and displacement ductility in reinforced concrete buildings, KSCE Journal of Civil Engineering 16(5): 759-770.

Belarbi, A. and Hsu, T.T.C., (1990). Stirrup stresses in reinforced concrete beams, ACI Structural Journal 87(5): 530-538.

CEB-FIP Model Code 1990: final draft (1991). Bulletin d'Information, Paris, July 203-205.

Cervera, M., Oliver, J. and Manzoli, O.L., (1996). A rate-dependent isotropic damage model for the seismic analysis of concrete dams, Earthquake Engineering and Structural Dynamics 25: 987-1010.

Delalibera, R.G., (2002). Análise teórica e experimental de vigas de concreto armado com armadura de confinamento, Dissertação de Mestrado, Escola de Engenharia de São Carlos, Universidade de São Paulo.

Daniell, J.E., Oehlers, D.J., Griffith, M.C., Mohamed Ali, M.S. and Ozbakkaloglu, T., (2008). The softening rotation of reinforced concrete members, Engineering Structures 30: 3159-3166.

Demir, A., Caglar, N., Ozturk, H. and Sumer, Y., (2016). Nonlinear finite element study on the improvement of shear capacity in reinforced concrete T-sections beams by an alternative diagonal shear reinforcement, Engineering Structures 120: 158-165.

EUROCODE 2 (1992). Design for concrete structures – Part 1: General rules and rules for buildings, Brussels, Belgium.

EUROCODE 8 (2004). Design of structures for earthquake resistance – Part 1: General rules, seismic actions and rules for buildings, Brussels, Belgium.

Figueiras, J.A., (1983). Ultimate load analysis of anisotropic and reinforced concrete plates and shells, Ph.D. Thesis, Department of Civil Engineering, University College of Swansea.

Flores-Lopes, J, (1993). Modelos de daño concentrado para la simulación numérica del colapso de pórticos planos, Revista Internacional de Métodos Numéricos para Cálculo y Diseño em Ingeniería 9(2): 123-139.

Kara, I.F. and Ashour, A.F., (2013). Moment redistribution in continuous FRP reinforced concrete beams, Construction and Building Materials 49: 939-948.

Kent, D.C. and Park, R., (1971). Flexural members with confined concrete, ASCE Proceedings 97(ST7): 1969-1990.

Ko, M.Y., Kim, S.W. and Kim, J.K., (2001). Experimental study of the plastic rotation capacity of reinforced high strength concrete beams, RILEM Materials and Structural Journal 34: 302-311.

La Borderie, C., (1991). Phenomenes unilateraux dans un materiau endommageable: modelisation et application a l'analyse de structures en béton, These de Doctorat (in french), Universite Paris, France.

Lee, T.K. and Pan, A.D.E., (2003). Estimating of relationship between tension reinforcement and ductility of reinforced concrete beams sections, Engineering Structures 25: 1057-1067.

Lopes, A.V., Lopes, S.M.R. and Carmo, R.N.F., (2012). Effects of the compressive reinforcement buckling on the ductility of RC beams in bending, Engineering Structures 37: 14-23.

Mazars, J., (1984). Application de la mechanique de l'endommagement au comportement non lineaire et à la rupture du béton de structure, These de Doctorat (in french), Universite Paris, France.

Nogueira, C.G., (2010). Desenvolvimento de modelos mecânicos, de confiabilidade e de otimização para aplicação em estruturas de concreto armado, Ph.D. Thesis (in portuguese), Escola de Engenharia de São Carlos, Universidade de São Paulo.

Nogueira, C.G., Venturini, W.S. and Coda, H.B., (2013). Material and geometric nonlinear analysis of reinforced concrete frames structures considering the influence of shear strength complementary mechanisms, Latin American Journal of Solids and Structures 10: 953-980.

Oehlers, D.J., Griffith, M.C. and Mohamed Ali, M.S., (2009). Ductility components and limits of FRP-plated structures, Construction and Building Materials 23: 1538-1543.

Oehlers, D.J., Visintin, P., Haskett, M. and Sebastian, W.M., (2013). Flexural ductility fundamental mechanisms governing all RC members in particular FRP RC, Construction and Building Materials 49: 985-997.

Perego, M, (1990). Danneggiamento dei material lapidei: leggi constitutive, analisis per elementi finiti ed applicazioni, Tesi di Laurea (in italian), Politecnico di Milano, Anno Accademico.

Pituba, J.J.C, (2003). Sobre a formulação de um modelo de dano para o concreto, Ph.D. Thesis (in portuguese), Escola de Engenharia de São Carlos, Universidade de São Paulo.

Saatcioglu, M. and Razvi, S.R., (1992). Strength and ductility of confined concrete, ASCE Journal of Structural Engineering 118(6): 1590-1607.

Ziara, M.M., Haldane, D. and Kuttab, A.S., (1995). Flexural behavior of beams with confinement, ACI Structural Journal 92(1): 103-114.